Nanoscience and Nanotechnology Letters
Vol. 1, 8–12, 2009

Fabrication, Structural Characterization, and Formation Mechanism of Ferroelectric $SrBi_2Ta_2O_9$ Nanotubes

Satyendra Singh and S. B. Krupanidhi*

Materials Research Centre, Indian Institute of Science, Bangalore 560012, India

A capillary-enforced template-based method has been applied to fabricate strontium bismuth tantalate ($SrBi_2Ta_2O_9$, SBTO) nanotubes (diameter ~ 200 nm) by filling SBTO precursor solution into the nanochannels of porous anodic aluminum oxide (AAO) templates. X-ray diffraction (XRD), field emission scanning electron microscopy (FE-SEM) and transmission electron microscopy (TEM) equipped with Energy-dispersive X-ray spectroscopy (EDX) have been employed to characterize the morphology, structure, and composition of as-prepared nanotubes. XRD and selected-area electron diffraction (SAED) investigations demonstrated that postannealed (650 °C for 1 h) SBTO nanotubes were polycrystalline with an orthorhombic perovskite crystal structure. The FE-SEM and TEM results showed that uniform length and diameter of SBTO nanotubes were obtained. The thickness of the SBTO nanotube walls was about 30 nm. High resolution TEM (HRTEM) analysis confirmed that the obtained SBTO nanotubes are made of randomly aligned nanoparticles 5–10 nm in size. EDX analysis demonstrated that stoichiometric $SrBi_2Ta_2O_9$ was formed. The possible formation mechanism of SBTO nanotubes in the AAO template is discussed.

Keywords: Nanofabrication, Nanotubes, Strontium Bismuth Tantalate, Electron Microscopy, Template.

1. INTRODUCTION

One-dimensional (1D) nanostructures, such as nanotubes, nanowires, and nanorods, of various materials have attracted considerable attention from scientific communities because they can play an important role in mesoscopic physics and nanoscale device fabrication, as they can be utilized as both nanoscale device elements and interconnections while retaining unique properties due to size confinement in the radial direction.[1–7] Recently, efforts have been made to synthesize and understand the growth of nanostructures of the ferroelectric materials because of the promise they show for the realization of nanoscale piezoelectric actuators and transducers, nonvolatile memory devices, and ultrasonic devices.[8–13] Ferroelectric random access memory has attracted much attention because of its advantages such as nonvolatile data retention, low power consumption, and fast read/write speed.[14] In this respect, lead zirconate titanate [$Pb(Zr_xTi_{1-x})O_3$, PZT], strontium bismuth tantalate ($SrBi_2Ta_2O_9$, SBTO), and $Bi_{1-x}La_xTi_3O_{12}$ are some promising candidates.[15–17] However, PZT has presented serious problems such as fatigue, leakage current, and aging, which may significantly degrade the performance of the material and the lifetime of the devices.[18, 19] SBTO with a layered structure[17] has emerged as a candidate for nonvolatile ferroelectric memory applications because of its excellent reliability properties such as fatigue and retention endurance.[20] The synthesis of ferroelectric SBTO nanostructures with controllable size and shape is critical not only in new nanoscale device applications but also from a fundamental point of view. Nanotubes of various materials have been synthesized by different methods,[21–23] among which, the sol–gel template approach offers a number of advantages in terms of tunability of the characteristic dimensions as well as better control of stoichiometry and higher flexibility.[24] Using the above method, nanotubes of various ferroelectric materials such as barium titanate, lead titanate, lead zirconate titanate [$Pb(Zr_{0.53}Ti_{0.47})O_3$], $BiFeO_3$ and $Ba_{0.6}Sr_{0.4}TiO_3$ have been already reported.[24–27] Morrison et al.[28] prepared the strontium bismuth tantalite nanotubes of diameter of about 800 nm using porous Si substrate. For the development of ferroelectric random access memories, the microstructure of grain boundaries and microstructural defects in SBTO materials is an important subject.[29] In this manuscript, we are reporting the synthesis of ferroelectric SBTO nanotubes about 200 nm in diameter using an anodic aluminum oxide (AAO) template, structural characterization of the

*Author to whom correspondence should be addressed.

 1941-4900/2009/1/008/005 doi:10.1166/nnl.2009.001

nanotubes, and the high resolution transmission electron microscopy (HRTEM) studies on the grain microstructure.

2. EXPERIMENTAL METHODS

For the preparation of SBTO nanotubes, initially, SBTO precursor solution was prepared by the sol–gel method. Strontium acetate hydrate [$Sr(CH_3COO)_2 \cdot xH_2O$, 99.99%, Aldrich], bismuth acetate [$Bi(CH_3COO)_3$, 99.99%, Aldrich], and tantalum ethoxide [$Ta(OC_2H_5)_5$, 99.98%, Aldrich], were used as the starting materials along with ethylene glycol and glacial acetic acid, which were used as the solvents. SBTO precursor solution was prepared by the sol–gel route, whereby strontium acetate and bismuth acetate were dissolved in ethylene glycol and glacial acetic acid with continuous stirring at 90 °C for 30 min. After cooling to room temperature, tantalum ethoxide was added drop-by-drop to the solution and stirred at 70 °C for 30 min. The pH value of the final solution was adjusted to ∼5 by adding ethylene glycol and glacial acetic acid. The solution was finally filtered through micro-fiber filter paper to obtain the final SBTO precursor solution. Nanotube arrays of SBTO were grown in the AAO templates by means of capillary force-induced filling. Commercially available AAO membranes (Whatman®, pore diameter: ∼200 nm and thickness: ∼60 μm) were used as the templates. Next, a few drops of the SBTO precursor solution were dropped on the cleaned Si substrate, and the AAO template was gently placed on the top of the precursor solution for 1 h at room temperature. Then template containing the precursor solution was dried at 150 °C for 2 h and subsequently heated at 650 °C for 1 h in air using a thermal annealing furnace to obtain the perovskite phase. The SBTO nanotubes were isolated after removal of the AAO templates by immersing them in 6 M NaOH solution at room temperature for 20 h. To retrieve reasonable quantities of nanotubes, the base solution was diluted in several steps with deionized distilled water. The isolated nanotubes were collected by centrifugation.

For powder X-ray diffraction (XRD) analysis, the template-free SBTO nanotube powder was nicely dispersed on the glass plate, and the XRD pattern was collected on a Philips PW3710 diffractometer (Cu-K_α radiation, 30 kV and 20 mA, $\lambda = 1.5406$ Å) from 20–65° at a scanning rate of 2°/min. The morphology of the as-prepared SBTO nanotubes was studied with a field emission scanning electron microscope (FE-SEM) (Sirion 200) operated at 10 kV. For SEM analysis, a thin layer of gold was sputtered onto the surface of the samples to reduce the charging effects. The morphology, selected-area electron diffraction (SAED), structure, and energy-dispersive X-ray spectroscopy (EDX) of the resulting SBTO nanotubes were examined by transmission electron microscope (TEM, Tecnai F30, equipped with EDX) operated at an accelerating voltage of 200 kV.

3. RESULTS AND DISCUSSION

Figure 1(a) shows a typical cross section FE-SEM image of an empty AAO template with pores parallel to each other and perpendicular to the surface of the AAO template. The inset in Figure 1(a) shows the top view of the unfilled AAO template. The diameters of the pores and the thickness of the AAO template were about 200 nm and 60 μm, respectively. Figure 1(b) shows the FE-SEM image of the nearly freestanding SBTO nanotubes after about

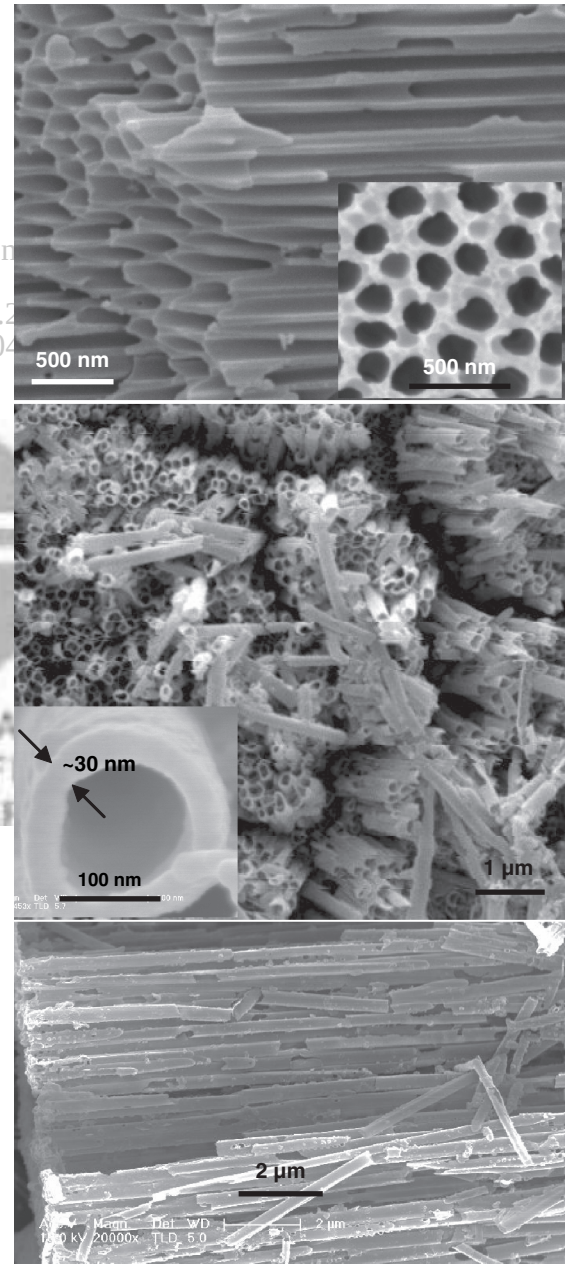

Fig. 1. FE-SEM images: (a) cross-section view of the unfilled AAO template—the inset shows the top view of the unfilled AAO template; (b) top view of the SBTO nanotubes after about 90% removal of AAO template—the inset shows the tip of an SBTO nanotube; and (c) aligned SBTO nanotubes after complete removal of the AAO template.

90% removal of the AAO template with NaOH solution. The micrograph clearly shows that as-synthesized SBTO nanotubes were hollow, roughly parallel to each other, and vertically oriented on the AAO template to form an array. The average diameter was ~200 nm, which is considerably smaller than the previous report.[28] The distribution of the nanotube diameters depends mainly on the pore dimensions in the template, as they mimic the distributions of the pore dimensions. The inset in Figure 1(b) shows the tip of an SBTO nanotube, which clearly demonstrates that the average thickness of the SBTO nanotube wall is about 30 nm, which is smaller than previously reported.[28] It was observed that outer diameter of these SBTO nanotubes was slightly smaller than the pore diameter in the template. This reduction in the diameter of the nanotube from the diameter of the pores is attributed to the shrinkage experienced by the SBTO nanotubes due to densification and dehydration involved in heat treatments. Figure 1(c) shows the self-aligned nanotubes after complete removal of the AAO template. The observed maximum length of the SBTO nanotubes was ~30 μm, whereas the expected maximum was ~60 μm (thickness of the template). The reason may be that pores in the template were not up to the full thickness of the template or were broken during the sonication treatment.

In order to confirm the crystallinity, phase purity, and structure of as-obtained SBTO nanotubes after annealing at 650 °C for 1 h, powder XRD analysis was carried out. Figure 2 shows the XRD pattern of the template-free SBTO nanotube powder, which was collected after several distillations of the NaOH solution. The XRD pattern of the SBTO nanotubes clearly shows that these are crystalline and no other impurity phase was observed. A diffuse halo can be observed around 20–40° from the glass slide used for making the sample. The observed XRD pattern of the

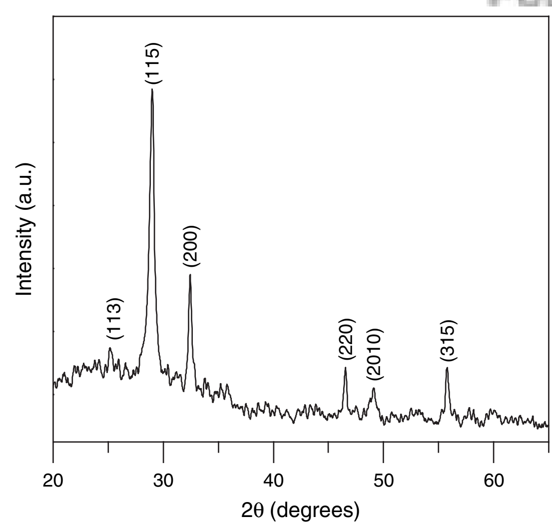

Fig. 2. XRD pattern of SBTO nanotube powder after complete removal of the AAO template.

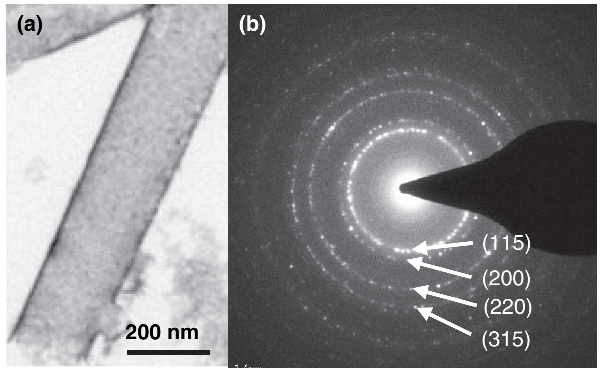

Fig. 3. TEM images: (a) an SBTO nanotube after complete removal of the AAO template; (b) corresponding SAED pattern.

SBTO nanotubes matched well with the orthorhombic perovskite phase of SBTO bulk (JCPDS Card No.: 49-0609).

Figure 3(a) shows the TEM image of an as-prepared SBTO nanotube after complete removal of the AAO template, and Figure 3(b) shows the corresponding SAED pattern. The difference in the contrast at the edges and the middle of the tube (Fig. 3(a)) clearly indicates that it is hollow, as the tube edges are dark compared to the middle portion of the tube due to more scattering. It is evident from this SAED pattern that these nanotubes are polycrystalline and the rings correspond to the (115), (200), (220), and (315) planes of the orthorhombic perovskite structure of SBTO. The d-spacings were calculated from the diameter of the bright circular rings observed in the electron diffraction pattern and were compared with the XRD data and the data available in the literature. The lattice d-spacings d_{115}, d_{200}, d_{220}, and d_{315} were about 3.05, 2.73, 1.92, and 1.61 Å respectively, which are in good agreement with the XRD results and with the open literature (JCPDS No. 49-0609).

The microstructure of the as-synthesized SBTO nanotubes was further investigated using HRTEM. Figure 4 shows a typical HRTEM image taken on the wall of an SBTO nanotube, which gives further insight into the details of the structure. It is evident from the HRTEM image in Figure 4 that the wall of the nanotube consists of a number of nanoparticles that are randomly oriented in the wall. The size of the nanoparticles in the walls was found to be in the 5–10 nm range, which is in good agreement with reported data for other functional complex oxide nanotubes.[25–27] The particles in the nanotubes were well-resolved, as one can see the clear lattice fringes in the HRTEM image, indicating that the SBTO nanotubes were well crystallized. If we carefully examine the HRTEM image, we can see some small regions that are not resolved, suggesting the presence of some pores in the SBTO nanotube. The distance between the parallel fringes is about 3.04 ± 0.01 Å, corresponding to the well-recognized d-spacings of (115) atomic planes of the orthorhombic structure of SBTO, which agrees with the values calculated from the SAED pattern, XRD, and open

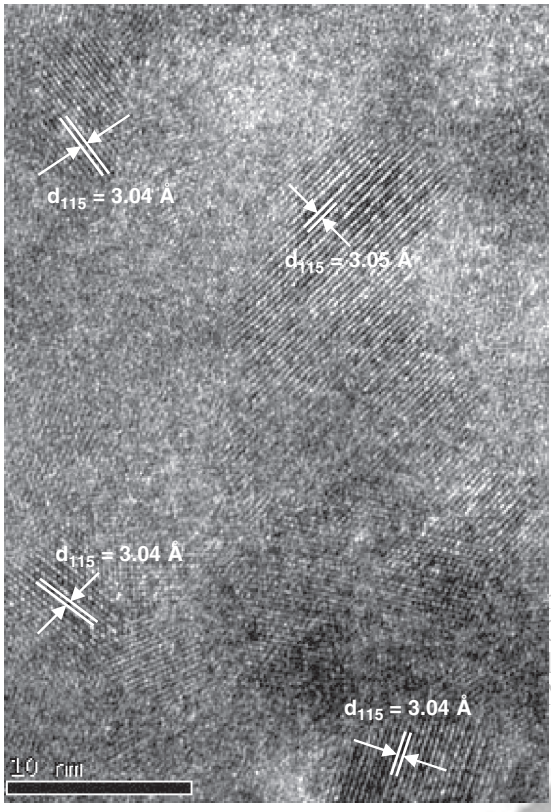

Fig. 4. HRTEM image of a single SBTO nanotube showing that it is composed of a number of randomly oriented nanoparticles.

literature (JCPDS No. 49-0609). The nanoparticles comprising the walls of the nanotubes in other oxide materials have been observed by various researchers and reported elsewhere.[25–27]

In order to confirm the chemical composition of the SBTO nanotubes, EDX spectroscopy were carried out at a number of selected positions on the nanotubes using the TEM. Figure 5 shows the EDX spectrum of an SBTO nanotube. It is clear from EDX spectrum that these nanotubes were composed of Sr, Bi, Ti, and O atoms. The average atomic ratios of Sr, Bi, Ti, and O in the nanotubes were around 0.0711, 0.1411, 0.1433 and 0.6415, which is very close to the nominal composition of $SrBi_2Ta_2O_9$. No emission lines from Al or other elements from the etching solution, reagent, or template appeared in this spectrum, thereby confirming the absence any impurities from the reactant or the template. The presence of the Cu peaks may be attributed to the Cu present in the TEM grid.

SBTO nanotubes were grown by sol-filling the pores of the AAO template with capillary force. The sol was drawn up into and filled the pores of the AAO template. Air in the pores and vapor from the sol were evaporated from the top surface of the AAO template. The possible formation mechanism of SBTO nanotube inside the pores of AAO template, based on a previous report,[30] is proposed here. Schematics of the possible formation mechanism of SBTO nanotubes inside the pores of the AAO template are shown in Figure 6 [(a) three-dimensional view of an AAO template, (b) setup for fabrication of SBTO nanotube, and (c) growth process of SBTO nanotube]. Initially, the template was put on the SBTO precursor solution as shown in Figure 6(b) because the solution is easier to fill into the pores of the template due to the capillary force. As the solvent evaporates from the surface and the concentration is enriched at the top of the pores, precipitation or gelation occurs first at the top of the pores on the AAO template surface exposed to the air and subsequently proceeds downward along the entire wall of the pores. The precursor solution consists of sol nanoparticles or nanoclusters homogeneously dispersed in the solvent. Such nanoclusters, which develop surface charges and form a double layer, can respond to an externally applied electric field or other nanoclusters.[30] When the surface of the AAO template is brought into contact with a sol, a surface charge and a double layer are formed on the surface of the AAO template. Therefore, when sols are drawn into the pore

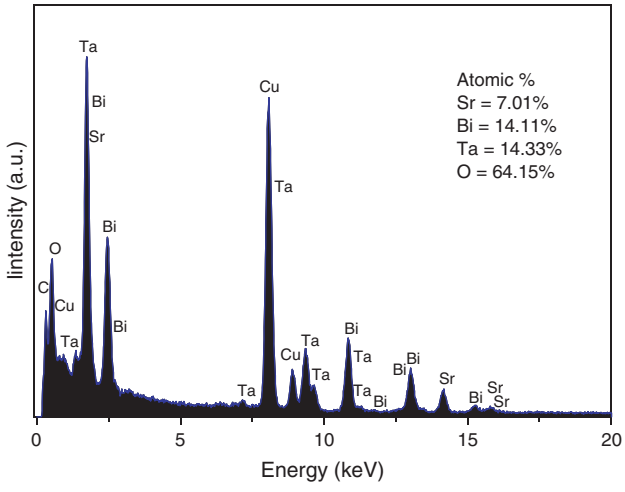

Fig. 5. EDX spectrum from an SBTO nanotube.

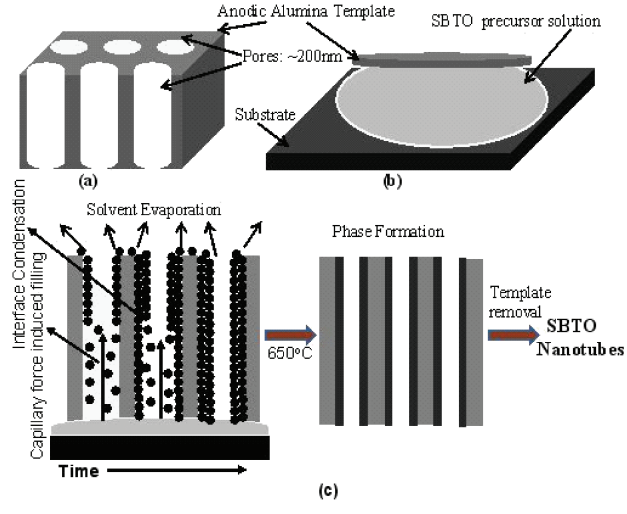

Fig. 6. A schematic diagram of the possible growth mechanism of SBTO nanotube in the AAO template.

channels of the AAO template, if the surface charges of nanoclusters in a sol and the surface of the AAO template are opposite, there will be an electrostatic attraction force, and the nanoclusters will preferentially deposit on the surface of the pore channel, resulting in the formation of nanotubes. This phenomenon has also been reported by Cao and Martin's group and explained in the same manner.[30–33]

4. CONCLUSIONS

In summary, SBTO nanotubes ~200 nm in diameter were fabricated successfully by the sol–gel method within the closely packed porous nanochannel alumina templates. Phase purity and crystalline orthorhombic perovskite phase formation of SBTO nanotubes were confirmed by the XRD and SAED patterns. EDX analysis demonstrated that stoichiometric $SrBi_2Ta_2O_9$ was formed. The walls of the nanotubes were found to be made of nanoparticles, which was confirmed from the HRTEM analysis. The average thickness of the nanotube walls was ~30 nm, and the nanoparticles comprising the wall were 5–10 nm in size. This facile method of preparing ferroelectric $SrBi_2Ta_2O_9$ nanotubes on a large scale may be important for many applications such as ferroelectric memory parts in future nanoscale devices.

References and Notes

1. Y. Chi and C. M. Lieber, *Science* 291, 851 (**2001**).
2. M. H. Huang, S. Mao, H. Feick, H. Q. Yan, Y. Y. Wu, H. Kind, E. Weber, R. Russo, and P. D. Yang, *Science* 292, 1897 (**2001**).
3. G. R. Patzke, F. Krumeich, and R. Nesper, *Angew. Chem., Int. Ed.* 41, 2446 (**2002**).
4. A. P. Alivisatos, *Science* 271, 933 (**1996**).
5. Y. Xia, P. Yang, Y. Sun, Y. Wu, B. Mayers, B. Gates, Y. Yin, F. Kim, and H. Yan, *Adv. Mater.* 15, 353 (**2003**).
6. J. Hu, T. W. Odom, and C. M. Lieber, *Acc. Chem. Res.* 32, 435 (**1999**).
7. C. N. R. Rao and M. Nath, *Dalton Trans.* 1 (**2003**).
8. C. D. Chandler, C. Roger, and M. J. Hampden-Smith, *Chem. Rev.* 93, 1205 (**1993**).
9. M. W. Chu, I. Szafraniak, R. Scholz, C. Harnagea, D. Hesse, M. Alexe, and U. Gosele, *Nat. Mater.* 3, 87 (**2004**).
10. J. Junquera and P. Ghosez, *Nature* 422, 506 (**2003**).
11. Y. Wang and J. J. Santiago-Aviles, *Nanotechnology* 15, 32 (**2004**).
12. A. Roelofs, I. Schneller, K. Szot, and R. Waser, *Appl. Phys. Lett.* 81, 5231 (**2002**).
13. Y. Luo, I. Szafraniak, N. D. Zakharov, V. Nagarajan, M. Steinhart, R. B. Wehrspohn, J. H. Wendorff, R. Ramesh, and M. Alexe, *Appl. Phys. Lett.* 83, 440 (**2003**).
14. A. Sheikholeslami and P. G. Gulak, *Proc. IEEE* 88, 667 (**2000**).
15. B. H. Park, B. S. Kang, S. D. Bu, T. W. Noh, J. Lee, and W. Jo, *Nature* 401, 682 (**1999**).
16. S. K. Dey, D. A. Payne, and K. D. Budd, *IEEE Trans. Ultrason. Ferroelectron. Freq. Control.* 35, 80 (**1988**).
17. K. N. Kim and Y. J. Song, *Microelectron. Reliab.* 43, 385 (**2003**).
18. J. F. Chang and S. B. Desu, *J. Mater. Res.* 9, 955 (**1994**).
19. W. L. Warren, D. Dimos, B. A. Tuttle, R. D. Nasby, and G. E. Pike, *Appl. Phys. Lett.* 65, 1018 (**1994**).
20. S. H. Oh, K. H. Noh, S. S. Lee, H. B. Kang, Y. H. Yang, K. N. Lee, S. K. Hong, and Y. J. Park, *J. Electrochem. Soc.* 151, F113 (**2004**).
21. O. G. Schmidt and K. Eberl, *Nature* 410, 168 (**2001**).
22. J. J. Urban, J. E. Spanier, O. Y. Lian, W. S. Yun, and H. Park, *Adv. Mater.* 15, 423 (**2003**).
23. C. R. Martin, *Science* 266, 1961 (**1994**).
24. B. A. Hernandez, C. Ki-Seog, E. R. Fisher, and P. K. Dorhout, *Chem. Mater.* 14, 480 (**2002**).
25. X. Y. Zhang, X. Zhao, C. W. Lai, J. Wang, X. G. Tang, and J. Y. Dai, *Appl. Phys. Lett.* 85, 4190 (**2004**).
26. S. Singh and S. B. Krupanidhi, *J. Nanosci. Nanotechnol.* 8, 335 (**2008**).
27. S. Singh and S. B. Krupanidhi, *Phys. Lett. A* 367, 356 (**2007**).
28. F. D. Morrison, L. Ramsay, and J. F. Scott, *J. Phys.: Condens. Matter* 15, L527 (**2003**).
29. X. Zhu, T. Zhu, Z. Liu, and N. Ming, *Appl. Phys. A* 72, 503 (**2001**).
30. Y. Wang and G. Cao, *J. Mater. Chem.* 17, 894 (**2007**).
31. B. B. Lakshmi, P. K. Dorhout, and C. R. Martin, *Chem. Mater.* 9, 857 (**1997**).
32. B. B. Lakshmi, C. J. Patrissi, and C. R. Martin, *Chem. Mater.* 9, 2544 (**1997**).
33. J. C. Hulteen and C. R. Martin, *J. Mater. Chem.* 7, 1075 (**1997**).

Received: 20 June 2008. Accepted: 10 July 2008.